Atmos. Chem. Phys. Discuss., 15, 25873–25905, 2015
www.atmos-chem-phys-discuss.net/15/25873/2015/
doi:10.5194/acpd-15-25873-2015

Atmospheric Chemistry and Physics Discussions

Water vapour variability in the high-latitude upper troposphere – Part 2: Impact of volcanic emissions

C. E. Sioris[1], J. Zou[2], C. T. McElroy[1], C. D. Boone[3], P. E. Sheese[2], and P. F. Bernath[3,4]

[1]Department of Earth and Space Science and Engineering, York University, Toronto, Canada, 4700 Keele St., Toronto, M3J 1P3, ON, Canada
[2]Department of Physics, University of Toronto, 60 St. George. St., Toronto, M5S 1A7, ON, Canada
[3]Department of Chemistry, University of Waterloo, 200 University Ave. W, Waterloo, N2L 3G1, ON, Canada
[4]Department of Chemistry & Biochemistry, Old Dominion University, 4541 Hampton Blvd., Norfolk, 23529, VA, USA

Received: 24 July 2015 – Accepted: 6 September 2015 – Published: 24 September 2015

Correspondence to: C. E. Sioris (csioris@sdcnlab.esse.yorku.ca)

Published by Copernicus Publications on behalf of the European Geosciences Union.

Abstract

The impact of volcanic eruptions on water vapour in the region of the high latitude tropopause is studied using deseasonalized time series based on observations by the Atmospheric Chemistry Experiment (ACE) water vapour sensors, namely MAESTRO (Measurements of Aerosol Extinction in the Stratosphere and Troposphere Retrieved by Occultation) and the Fourier Transform Spectrometer (ACE-FTS). The three eruptions with the greatest impact on the high latitude upper troposphere during the time frame of this satellite-based remote sensing mission are chosen. The Puyehue-Cordón Caulle volcanic eruption in June 2011 was the most explosive eruption in the past 24 years and resulted in an observed (50 ± 12) % increase in water vapour in the southern high-latitude upper troposphere in July 2011 that persisted into September 2011. A pair of Northern Hemisphere volcanoes, namely Eyjafjallajökull and Nabro, erupted in 2010 and 2011 respectively, increasing water vapour in the upper troposphere at northern high latitudes significantly for a period of ∼ 3 months following each eruption. Both had a volcanic explosivity index of 4. Nabro led to a statistically significant increase of ∼ 1 ppm in lower stratospheric (13.5–15.5 km) water vapour at northern high-latitudes (60–90° N) in September 2011, when the brunt of its plume arrived in the Arctic. These findings imply that steam emitted into the high-latitude, upper troposphere during volcanic eruptions must be taken into account to properly determine the magnitude of the trend in water vapour over the last decade.

1 Introduction

Water vapour is the most abundant volcanic gas, comprising over 80 % by volume (Pinto et al., 1989). Water vapour in the tropopause region is particularly effective at trapping outgoing longwave radiation emitted by the surface (Solomon et al., 2010). Steam emitted by volcanic eruptions can have a lasting climatic impact when the water vapour reaches the stratosphere. Enhanced stratospheric water vapour (up to

ACPD
15, 25873–25905, 2015

64 ppmv) was observed using a frost-point hygrometer in the plume originating from the 18 May 1980 eruption of Mount St. Helens (Murcray et al., 1981) near an altitude of 20 km four days later. Since then, there has been little evidence of large or long-lived stratospheric water vapour enhancements, although in theory (e.g. Glaze et al., 1997; Arfeuille, 2012), moderate enhancements are possible, particularly for tropical eruptions where entrainment of tropospheric moisture adds to the contribution from the magmatic water. Stratospheric Aerosol and Gas Experiment (SAGE) II enhancements following the eruption of Mount Pinatubo may be artificial given that when Halogen Occultation Experiment (HALOE) began observing in late 1991, months after eruption, SAGE II continued to observe water vapour enhancements while HALOE (Fueglistaler et al., 2013) and UARS/MLS (Elson et al., 1996) were not observing enhanced stratospheric water vapour. However, both Stenke and Grewe (2005) and Joshi and Shine (2003) noted a short-lived increase in stratospheric water vapour (of > 1 ppm) observed by frostpoint hygrometers over Boulder, Colorado in early 2002 and considered it to be a consequence of increased water vapour at the tropical tropopause due to local warming by Pinatubo aerosols (Considine et al., 2001). These anomalous water vapour enhancements in early 1992 remain in the updated Boulder data (Hurst et al., 2011), specifically at 24–26 km. Upper tropospheric water vapour (UTWV) was observed to decrease following the Pinatubo eruption due to global cooling below the tropopause (Soden et al., 2002). Joshi and Shine (2003) and Stenke and Grewe 2005) also related < 1 ppm enhancements of stratospheric water vapour measured by frost-point hygrometers in 1982 to the eruption of El Chichón. The largest eruption of the past two centuries is Tambora in 1815, whose volcanic explosivity index (VEI) was 7, compared to a VEI of 6 for the 1991 Mount Pinatubo eruption and is estimated to have more than doubled stratospheric water vapour (Glaze et al., 1997, and reference therein) at least initially. Water vapour is consumed by reaction with SO_3 in the final step of sulphuric acid formation and also condenses on the resulting sulphuric acid particles so that local humidity can decrease even for larger injections of water into the stratosphere such as produced by Toba 70 000 years ago if the eruption is sulphur-rich (Bekki et al.,

ACPD
15, 25873–25905, 2015

1996). Water can enter the stratosphere as ice coatings on volcanic ash (e.g. Pieri et al., 2002). With the typically low relative humidity of the stratosphere, this ice can readily vaporize before the particles fall out of the stratosphere.

Three recent volcanic eruptions which produced obvious upper tropospheric water vapour enhancements: Puyehue-Cordón Caulle (June 2011), Nabro (June 2011), and Eyjafjallajökull (April 2010) are studied here. Nabro is also shown to cause a significant increase in lower stratospheric water vapour at northern high latitudes, albeit for a short period (on the order of a few months), consistent with the timescale over which extratropical lower stratospheric water vapour remains above the tropopause (Wilcox et al., 2012). While the climatic impact of enhanced water vapour due to the Puyehue eruption is shown to be minor, particularly given the short period of this volcanic enhancement, such increases are relevant for UTWV trend studies, particularly if an eruption occurs near the start or end of the period under consideration. Currently, trends in UTWV are not known for high latitudes (Hartmann et al., 2013). However, the main focus of this work is on improving our understanding of UTWV variability at high latitudes and the role of volcanic emissions relative to other dynamical and thermodynamic processes in this region (see companion paper: Sioris et al., 2015).

2 Methods

SCISAT was launched in 2003 (Bernath et al., 2005) and the Atmospheric Chemistry Experiment (ACE) datasets begin in February 2004. The satellite bears two limb sounders measuring water vapour that both rely on the solar occultation technique: measurements of Aerosol Extinction in the Stratosphere and Troposphere Retrieved by Occultation (MAESTRO) and the Fourier Transform Spectrometer (ACE-FTS) as well as an Imager (Bernath et al., 2005) which provides aerosol extinction measurements (e.g. Vanhellemont et al., 2008) that can be directly compared with those retrieved from MAESTRO observations. MAESTRO is currently the only satellite instrument capable of simultaneously measuring vertical profiles of both water vapour and extinction

ACPD
15, 25873–25905, 2015

by fine aerosols (Sioris et al., 2010a) down to the mid-troposphere. The MAESTRO water vapour retrieval relies on the 940 nm absorption band and is described by Sioris et al. (2010b) and updated recently (Sioris et al., 2015). Figures 1 and 2 present the validation of MAESTRO water vapour. MAESTRO is seen to have less scatter than ACE-FTS below 6.5 km. Between 6 and 19.5 km, the median of the relative differences between MAESTRO and ACE-FTS of their individual collocated profiles is $< 20\,\%$, which is also true only for MIPAS IMK data (Stiller et al., 2012) considering the other UTLS water vapour data products compared in Fig. 2. However, due to the relatively large noise in the MAESTRO lower stratospheric water vapour data (Fig. 2), the scatter in the relative differences between individual coincident ACE-FTS and MAESTRO profiles of is on the order of $\sim 35\,\%$, whereas those between ACE-FTS and other atmospheric sounders are typically on the order of $\sim 10\,\%$ in this region.

Sioris et al. (2010b) found a weak sensitivity of the water vapour retrieval to significant perturbations in aerosol extinction. As discussed in Sioris et al. (2010b), the weaker sensitivity of MAESTRO water vapour to aerosol extinction relative to other solar occultation instruments which have used this absorption band, namely Polar Ozone and Aerosol Measurement (POAM) III and SAGE II, is due to the availability of "off" wavelengths (i.e. with minimal absorption by water vapour) on both sides of the water vapour band, which neither of these other instruments incorporated into their channel selection. This issue is also true for SAGE III (Thomason et al., 2010) with neighbouring channels at 869 and 1021 nm, but to a lesser extent than for SAGE II.

ACE-FTS gridded version 3.5 data are used in the study (Boone et al., 2013) and have been validated as discussed in the companion paper. Over the microwindows used to retrieve water vapour from ACE-FTS spectra, absorption by this trace gas is completely uncorrelated with the spectrally smooth aerosol extinction signature. The insensitivity to aerosol extinction of water vapour retrieved from high-resolution solar occultation spectra using microwindows is well known (e.g. Rinsland et al., 1994; Michelsen et al., 2002; Steele et al., 2006; Uemera et al., 2005). The ACE-FTS algorithm uses this microwindow technique and uses a slope term in each microwindow

ACPD
15, 25873–25905, 2015

(Boone et al., 2005). Over each microwindow used to retrieve water vapour, no higher order baseline terms are necessary. The complete insensitivity to aerosol extinction is an advantage of the microwindow technique relative to the band-integrated approach used in the MAESTRO water vapour retrieval. This advantage is possible due to the high spectral resolution of ACE-FTS which assists in separating the continuum level, which is monotonic over a microwindow, from the deep absorption lines due to light, gas phase molecules such as H_2O.

The monthly tropopause height is defined by the lower of the lowest local minimum above 5 km or the lowest height above 5 km at which the lapse rate is $< 2\,\mathrm{K\,km^{-1}}$ in monthly median temperatures from the Global Environmental Multiscale (GEM) regional weather forecast model (Laroche et al., 1999). Further details are given in the companion paper.

To obtain a water vapour relative anomaly time series for the UTLS, the method follows that of Sioris et al. (2015). The monthly climatology, used to deseasonalize the time series, is generated by averaging the monthly medians over the populated years, with a minimum sample size of 20 observations per altitude bin per month. Between 5.5 and 19.5 km using 1 km vertical bins, climatological profiles are obtained for all calendar months except April, June, August, and December at northern high latitudes (60–90° N) and all months except February, June, October, and December at southern high-latitudes (60–90° S), as ACE does not sample these regions in these months.

3 Results

3.1 Puyehue-Cordón Caulle

The Puyehue-Cordón Caulle volcano erupted in early June 2011. Figure 3 shows MAESTRO time series in the UT region, indicating an anomalous increase in water vapour mixing ratio in July 2011, increasing relative to May 2011, whereas in a typical year, the mixing ratio can be seen to decrease from May to September as part of the strong sea-

ACPD
15, 25873–25905, 2015

sonal cycle. Note that the upper troposphere is not warmer in July or August of 2011 than in May 2011 according to GEM (Global Environmental Multiscale) model analysis temperatures (Laroche et al., 1999) sampled at the locations of atmospheric chemistry experiment (ACE) observations, and yet it is more humid. Figure 4 is a deseasonalized version of Fig. 3, illustrating a large increase in high latitude UTWV in the austral summer of 2011 that significantly biases (at the 1σ level) the inferred decadal trend at 8.5 km. In austral summer, the southern high-latitude observations occur from early July to austral spring equinox covering latitudes from 60 to 81° S with a two day absence in late August. Note that the spatiotemporal sampling repeats annually for ACE as illustrated by Randel et al. (2012). The typical "stratospheric" values (< 10 ppm) that annually appear in September at 7.5 and 8.5 km did not appear in September 2011. Figure 5 shows a statistically significant increase in UTWV in the 40–60° S latitude band as well for July 2011 relative to a normal year (July 2012), and no significant increase above 10 km. ACE samples the 40–60° S band in the first 12 days of the month and then samples the 60–90° S band (actually 60–66° S) for the remainder of the month. The large increase in water vapour at 8 km is present in both latitude bands. The consistency of these ratio profiles between middle and high southern latitudes provides evidence of the poleward transport of UTWV emitted by the powerful eruption (VEI of 5) of the Puyehue-Cordón Caulle volcano (http://www.volcano.si.edu/volcano.cfm?vn=357150).

The anomalous, sharp peak in monthly median aerosol extinction in the southern high-latitude upper troposphere observed by measurements of aerosol extinction in the stratosphere and troposphere retrieved by occultation (MAESTRO, McElroy et al., 2007) (not shown) and ACE-Imager (Fig. 6) confirms Puyehue aerosol observations by other satellite instruments (Vernier et al., 2013; Theys et al., 2014) and corroborates the volcanic origin of the water vapour enhancement. While there is a local maximum in relative humidity vs. altitude in the southern high-latitude upper troposphere in July 2011, the monthly median relative humidity is only ~ 50 % based on MAESTRO water vapour and co-located GEM model analysis temperatures (Laroche et al., 1999), meaning that most of the water emitted from the volcanic eruption will tend to remain in the vapour

ACPD
15, 25873–25905, 2015

phase as it is advected to the southern high-latitude upper troposphere (see Fig. 7). Furthermore, the earliest available observations of the volcanic plume by MAESTRO and ACE-Imager (at 42.3° S, 70.7° W on 1 July 2011) indicate a fine aerosol plume peaking at 9.5 km (spanning 8.5–10.5 km) with relative humidity obtained using MAESTRO water vapour peaking at 67 ± 14 % at 8.7 km (Fig. 7), establishing that the upper troposphere was not saturated less than 4 weeks after the eruption. Considering both the ACE-FTS (Bernath et al., 2005) and MAESTRO measurements, the largest relative volcanic enhancements in water vapour occur at 7.5–9.5 km in July 2011, where a doubling occurs relative to normal mixing ratios for that month (see Fig. 8). By August 2011, the relative anomaly remains of similar magnitude throughout the upper troposphere, and is statistically significant (1σ) at 7.5–8.5 km (seen by both instruments) and September is enhanced slightly, particularly at 7.5 km. In July 2011, relative humidity of 100 % with respect to ice (see Murray, 1967) was reached in some profile observations in the southern high-latitude upper troposphere with the corresponding MAESTRO aerosol extinction observations indicating a thin plume of fine particles. Thus, ice-coated tropospheric aerosols are inferred to be present for these cases.

The large enhancement in UTWV at southern high latitudes in July 2011 however does not significantly change the cooling rate at the surface (see Appendix A for details of the method).

3.2 Nabro

Nabro erupted on 13 June 2011, but the water vapour enhancement at northern high latitudes in July 2011 was minor. The ACE instruments do not observe northern high latitudes in August but by September 2011, enhanced water vapour (significant relative to quadrature-sum of the interannual standard deviation and the September 2011 standard error) was observed at 10.5–11.5 km by both instruments, with MAESTRO observing the peak of the enhancement at 10.5 km and ACE-FTS at 11.5 km (Fig. 9). Both instruments agreed on the magnitude of the enhancement near this ∼ 11 km peak (51 ± 13 %, Fig. 9). The brunt of the lower stratospheric aerosol enhancement

ACPD
15, 25873–25905, 2015

from Nabro arrived in the Arctic from mid-latitudes by September 2011 riding along the 420 K isentrope and thus descending a couple of kilometres in altitude (Bourassa et al., 2012). Figure 10 shows a significant water vapour anomaly of +30 % at northern mid-latitudes (30–60° N) peaking sharply at 13.5 km during summer 2011, while no other altitude level shows a significant positive anomaly. This anomaly peak height was consistent between July and September of 2011 and the anomaly decreased from 2.4 to 1.8 ppm between these two months. Individual ACE-FTS observations were examined and > 10 ppm of water vapour was not found in the stratosphere in any profile observation based on thermal tropopause heights. The thermal tropopause height definition was chosen for the mid-latitude data to be more conservative about locating the water vapour enhancements in the stratosphere in contrast to the general definition used in this work (see Sect. 2). The latitudinal sampling in 2011 at mid-latitudes was similar to other years in July and September with an average sampled latitude of 50° N.

The positive anomaly at northern high latitudes (60–90° N) at 12.5–13.5 km is the largest on record at this altitude for any calendar month in this latitude band ($N = 63$) for both MAESTRO and ACE-FTS. The monthly median tropopause height is 10.5 km in September 2011, yet Nabro appeared to increase water vapour by 30–50 % at 12.5 km according to both ACE sensors for that month relative to their respective climatological values. Near-IR ACE-Imager aerosol extinction observations indicate an aerosol layer also peaking at 13.5 km with very little variability at that altitude (Fig. 11). The low variability provides evidence that the plume had spread zonally in the northern high-latitude region three months after eruption. Figure 12 illustrates the tropopause height of each of the northern high-latitude ACE observations in September 2011. A tropopause height of 12.5 km occurs 1 % of the time and never above that altitude in this month.

In the high-latitude regions for the months affected by the three eruptions studied in this work, only September 2011 at northern high latitudes had biased sampling. We determined ACE-FTS water vapour anomalies for September in a narrower band (60–72° N) where the sampling is more uniform from year-to-year than for 60–90° N.

ACPD
15, 25873–25905, 2015

The observed enhancement profile in the two latitude bands are consistent within the uncertainties of the enhancement for the 60–90° N band (Fig. 13). Again, two sources of uncertainty are considered at each altitude:

1. the interannual variability, measured by the standard deviation of the water vapour volume mixing ratio (VMR) over all Septembers, and
2. the variability within the month of September 2011.

Given the consistency of ACE-FTS water vapour between the two high-latitude bands, we rely on the enhancement profile over the full high-latitude region (60–90° N) since it has a larger sample size. According to ACE-FTS, there is an enhancement in September 2011 relative to all other Septembers between 10.5 and 19.5 km. MAESTRO measurements of this enhancement are consistent with the enhancement observed by ACE-FTS but have larger uncertainties in the lower stratosphere as expected. The enhancement observed by ACE-FTS is 0.7 ± 0.4 ppm at 13.5 km and decreases steadily with altitude to 0.4 ± 0.3 at 15.5 km. MAESTRO does not see a significant enhancement above 11.5 km when 1 km vertical binning is used. However, when the water vapour VMR anomaly is calculated for a 3 km bin spanning 13.0–16.0 km and the uncertainties over the three 1 km bins are combined in root-sum-square fashion, the anomaly is 1.1 ± 0.8 ppm in this 3 km partial column. Unfortunately, the sample sizes for October and November of 2011 are currently inadequate. In January 2012, both instruments measured the highest water vapour VMR at 16.5 km for any January at northern high-latitudes: 4.6 and 4.7 ppm for MAESTRO and ACE-FTS respectively. These VMRs are statistically significant enhancements for both instruments (relative to 1σ of interannual variability), with ACE-FTS detecting an enhancement of 0.3 ± 0.2 ppm. This stratospheric water vapour enhancement is identical to the enhancement of 0.3 ± 0.2 ppm determined using ACE-FTS data for September 2011 at 16.5 km (Fig. 13) and corresponds to a subtle yet statistically significant anomaly in aerosol extinction (monthly mean minus monthly median MAESTRO aerosol extinction at 525 nm exceeds one standard error of the mean, considering the 12–30 km range in 1 km increments) that

ACPD
15, 25873–25905, 2015

spans 15.5–17.5 km, indicating a vertical correlation of the water vapour enhancement to a recent vertically-localized aerosol extinction enhancement. As the contribution of the volcanic aerosol diminishes due to sedimentation and diffusion, the median and average come into closer agreement as the aerosol extinction observations becomes more symmetrically distributed about the mean as is observed at all overlying altitudes (e.g. 18–30 km). As none of the observations in January 2012 at 15.5 km (N = 127) had a temperature below 195 K, polar stratospheric clouds can be ruled out as an alternate cause of aerosol enhancement there and tropospheric clouds could also be ruled out since the highest observed tropopause was 12.5 km. In May 2012, there are only significant positive anomalies of water vapour at 18.5–19.5 km observed by both instruments that correspond with a statistically insignificant MAESTRO 525 nm aerosol extinction enhancement. While the Nabro aerosol perturbation may have descended, there is also the possibility that the water vapour enhancement at 18.5–19.5 km is not due to Nabro. As this is the most recent available May, the anomaly may simply be related to increasing stratospheric water vapour from CH_4 breakdown as ACE-FTS shows an increasing trend (2004–2012) at both 18.5 and 19.5 km. Thus, we conclude that evidence for enhanced lower stratospheric water vapour due to Nabro is only present up until January 2012 in the ACE sensor datasets.

3.3 Eyjafjallajökull

Eyjafjallajökull began erupting on 14 April 2010 below 210 m of glacial ice (Magnússon et al., 2012), reaching an altitude of 10 km (Gudmundsson et al., 2012). ACE does not cover northern high latitudes in April, but in May 2010, MAESTRO and ACE-FTS both see statistically significant enhancements in water vapour at 8.5–9.5 km (Fig. 14). In fact, at 9.5 km, the (69 ± 10) % anomaly in May 2010 is the largest anomaly at this altitude in any of the 63 months that sample northern high latitudes in either dataset. The stated statistical significance considers the respective interannual variability for the month of May and the respective relative standard error for May 2010 for each dataset. The monthly mean tropopause height in May 2010 is 10.5 km but some individual ob-

ACPD
15, 25873–25905, 2015

servations have a tropopause height as high as 11.5 km. The peak of the Eyjafjallajökull aerosol layer is at 7.5 km approximately one month after eruption (Fig. 15). Figure 15 reveals an upper tropospheric aerosol layer that is not homogeneously spread throughout northern high latitudes based on differences between MAESTRO 560 nm May 2010 mean and median aerosol extinctions and the fact that both peak at 7.5 km. The ACE-Imager NIR data at northern high latitudes in May 2010 confirm an aerosol layer at 7.5 ± 0.5 km (not shown). The Arctic oscillation would be expected to increase water vapour by < 8 % at 8.5–9.5 km in May 2010 according to the regression using year-round monthly-sampled data as determined in the companion paper (Sioris et al., 2015) and is thus insufficient to explain the increase. Also, although dehydrated and rehydrated layers were observed in the 2010 winter (Khaykin et al., 2013), water vapour in the upper troposphere and lower stratosphere (UTLS, 5–20 km) in the northern high latitude region in March 2010 was normal according to both MAESTRO and ACE-FTS. ACE does not sample northern high latitudes in June, but in July, significant enhancements of water vapour of 22 and 45 % remained only at the tropopause (11.5 km) according to MAESTRO and ACE-FTS, respectively. This water vapour enhancement coincides with the top portion of an aerosol layer that spans 7.5 to 11.5 km according to July 2010 NIR Imager observations.

4 Discussion

In the time span of 14 months (April 2010 to June 2011), three eruptions with VEI ≥ 4 occurred that had a period of significant enhanced UTWV of ∼ 3 months, leading to monthly median increases of up to 50 %. While each of these three impacted the high-latitude, upper troposphere in the hemisphere of the eruption, two of the eruptions did not occur at high latitudes. Nabro is a tropical volcano and Puyehue is a southern mid-latitude volcano. Enhancements in the lower stratosphere and the high-latitude upper troposphere are more readily detected because of the low background VMR of water vapour in these regions. When the eruption occurs during the dry half of the

ACPD
15, 25873–25905, 2015

year (late autumn to early spring), the relative perturbation to the upper troposphere is even larger and can last longer due to reduced rainout. Thus the timing and location of the Puyehue eruption were favourable for detecting its water vapour enhancement. ACE-FTS and MAESTRO indicate a ∼ 1 ppm increase in stratospheric water vapour at ∼ 14 km at northern high latitudes due to the eruption of Nabro. Nabro may be a special case because the monsoon aided the cross-tropopause flux of volcanic ejecta (Bourassa et al., 2012), including ash subsequently coated in ice during tropospheric ascent. Eyjafjallajökull is likely a special case since the volcano was below > 200 m of glacial ice, some of which was vaporized in the process and rose in the eruption column. Other recent eruptions such as Kasatochi, which generated much more SO_2 and whose plumes went higher into the atmosphere than Nabro (and Eyjafjallajökull), were observed to have little impact on stratospheric water vapour. It is interesting to note that Eyjafjallajökull (Sears et al., 2013) and Puyehue (Pumphrey et al., 2015) emitted relatively little SO_2 considering their VEI values, thereby allowing less volcanic water vapour to be consumed by the reaction which converts SO_3 to sulphuric acid and also reducing the probability of water uptake by sulphate aerosol. Volcanic emissions are known to be more variable in terms of SO_2 than water vapour (Pinto et al., 1989).

Finally, solar occultation instruments, particularly those operating at visible and near-infrared wavelengths, have the unique capability among space-borne instruments to simultaneously observe vertical profiles of aerosol extinction and water vapour in the UTLS to provide an understanding of the impact of volcanic emissions on the water vapour budget and trends in water vapour.

Appendix: Cooling rate differences

Cooling rate vertical profiles are calculated for July 2011 using MODTRAN5.2 (e.g. Bernstein et al., 1996) assuming an Antarctic surface altitude of 2.5 km, tropospheric monthly medians of the GEM analysis temperatures (to the surface) and aerosol extinction profiles from MAESTRO at 560 nm down to 5 km and two water vapour cases:

ACPD
15, 25873–25905, 2015

1. using MAESTRO July climatological median water vapour between 6.5 and 9.5 km, and

2. with the increase in water vapour over this altitude range due to the Puyehue eruption determined by multiple linear regression with the Antarctic oscillation index (Mo, 2000) (http://www.cpc.ncep.noaa.gov/products/precip/CWlink/) plus a constant being the other basis functions. A monthly timestep is used with the Puyehue eruption basis function having a value of 1 for July–August 2011 and 0 in all other months for the purpose of the regression analysis.

Acknowledgements. The ACE mission is supported primarily by the Canadian Space Agency. David Plummer (Environment Canada) is acknowledged for his encouragement to perform cooling rate simulations for the Puyehue eruption. We appreciate the availability of the AO and AAO indices from the National Oceanic and Atmospheric Administration.

References

Arfeuille, F.: Impacts of large volcanic eruptions on the stratosphere and climate, DSc dissertation, EZT Zurich, Zurich, 104 p., 2012.

Bekki, S., Pyle, J. A., Zhong, W., Toumi, R., Haigh, J. D., and Pyle, D. M.: The role of microphysical and chemical processes in prolonging the climate forcing of the Toba eruption, Geophys. Res. Lett., 23, 2669–2672, 1996.

Bernstein, L. S., Berk, A., Acharya, P. K., Robertson, D. C., Anderson, G. P., Chetwynd, J. H., and Kimball, L. M.: Very narrow band model calculations of atmospheric fluxes and cooling rates, J. Atmos. Sci., 53, 2887–2904, 1996.

Boone, C. D., Nassar, R., Walker, K. A., Rochon, Y., McLeod, S. D., Rinsland, C. P., and Bernath, P. F.: Retrievals for the atmospheric chemistry experiment Fourier-transform spectrometer, Appl. Optics, 44, 7218–7231, 2005.

Boone, C. D., Walker, K. A., and Bernath, P. F.: Version 3 retrievals for the atmospheric chemistry experiment fourier transform spectrometer (ACE-FTS), in: The Atmospheric Chemistry Experiment ACE at 10: A Solar Occultation Anthology, edited by: Peter, F. and Bernath, A., Deepak Publishing, Hampton, VA, USA, 2013.

ACPD

15, 25873–25905, 2015

Bourassa, A. E., Robock, A., Randel, W. J., Deshler, T., Rieger, L. A., Lloyd, N. D., Llewellyn, E. J., and Degenstein, D. A.: Large volcanic aerosol load in the stratosphere linked to Asian monsoon transport, Science, 337, 78–81, 2012.

Considine, D. B., Rosenfield, J. E., and Fleming, E. L.: An interactive model study of the influence of the Mount Pinatubo aerosol on stratospheric methane and water trends, J. Geophys. Res., 106, 27711–27727, 2001.

Elson, L. S., Read, W. G., Waters, J. W., Mote, P. W., Kinnersley, J. S., and Harwood, R. S.: Space–time variations in water vapor as observed by the UARS microwave limb sounder, J. Geophys. Res., 101, 9001–9015, 1996.

Fueglistaler, S., Liu, Y. S., Flannaghan, T. J., Haynes, P. H., Dee, D. P., Read, W. J., Remsberg, E. E., Thomason, L. W., Hurst, D. F., Lanzante, J. R., and Bernath, P. F.: The relation between atmospheric humidity and temperature trends for stratospheric water, J. Geophys. Res.-Atmos., 118, 1052–1074, doi:10.1002/jgrd.50157, 2013.

Glaze, L. S., Baloga, S. M., and Wilson, L.: Transport of atmospheric water vapor by volcanic eruption columns, J. Geophys. Res., 102, 6099–6108, 1997.

Gudmundsson, M. T., Thordarson, T., Höskuldsson, Á., Larsen, G., Björnsson, H., Prata, F. J., Oddsson, B., Magnússon, E., Högnadóttir, T., Petersen, G. N., Hayward, C. L., Stevenson, J. A., and Jónsdóttir, I.: Ash generation and distribution from the April–May 2010 eruption of Eyjafjallajökull, Iceland, Sci. Rep., 2, 572, doi:10.1038/srep00572, 2012.

Hartmann, D. L., Klein Tank, A. M. G., Rusticucci, M., Alexander, L. V., Brönnimann, S., Charabi, Y., Dentener, F. J., Dlugokencky, E. J., Easterling, D. R., Kaplan, A., Soden, B. J., Thorne, P. W., Wild, M., and Zhai, P. M.: Observations: atmosphere and surface, in: Climate Change 2013: The Physical Science Basis, Contribution of Working Group I to the Fifth Assessment Report of the Intergovernmental Panel on Climate Change, edited by: Stocker, T. F., Qin, D., Plattner, G.-K., Tignor, M., Allen, S. K., Boschung, J., Nauels, A., Xia, Y., Bex, V., and Midgley, P. M., Cambridge University Press, Cambridge, UK, and New York, NY, USA, 2013.

Hurst, D. F., Oltmans, S. J., Vömel, H., Rosenlof, K. H., Davis, S. M., Ray, E. A., Hall, E. G., and Jordan, A. F.: Stratospheric water vapor trends over Boulder, Colorado: analysis of the 30 year Boulder record, J. Geophys. Res., 116, D02306, doi:10.1029/2010JD015065, 2011.

Joshi, M. M. and Shine, K. P.: A GCM study of volcanic eruptions as a cause of increased stratospheric water vapor, J. Climate, 16, 3525–3534, 2003.

ACPD
15, 25873–25905, 2015

Khaykin, S. M., Engel, I., Vömel, H., Formanyuk, I. M., Kivi, R., Korshunov, L. I., Krämer, M., Lykov, A. D., Meier, S., Naebert, T., Pitts, M. C., Santee, M. L., Spelten, N., Wienhold, F. G., Yushkov, V. A., and Peter, T.: Arctic stratospheric dehydration – Part 1: Unprecedented observation of vertical redistribution of water, Atmos. Chem. Phys., 13, 11503–11517, doi:10.5194/acp-13-11503-2013, 2013.

Laroche, S., Gauthier, P., St-James, J., and Morneau, J.: Implementation of a 3-D variational data assimilation system at the Canadian meteorological centre, Part II: the regional analysis, Atmos. Ocean, 37, 281–307, 1999.

Magnússon, E., Gudmundsson, M. T., Roberts, M. J., Sigurðsson, G., Höskuldsson, F., and Oddsson, B.: Ice-volcano interactions during the 2010 Eyjafjallajökull eruption, as revealed by airborne imaging radar, J. Geophys. Res., 117, B07405, doi:10.1029/2012JB009250, 2012.

McElroy, C. T., Nowlan, C. R., Drummond, J. R., Bernath, P. F., Barton, D. V., Dufour, D. G., Midwinter, C., Hall, R. B., Ogyu, A., Ullberg, A., Wardle, D. I., Kar, J., Zou, J., Nichitiu, F., Boone, C. D., Walker, K. A., and Rowlands, N.: The ACE-MAESTRO instrument on SCISAT: description, performance, and preliminary results, Appl. Optics, 46, 4341–4356, 2007.

Michelsen, H. A., Manney, G. L., Irion, F. W., Toon, G. C., Gunson, M. R., Rinsland, C. P., Zander, R., Mahieu, E., Newchurch, M. J., Purcell, P. N., Remsberg, E. E., Russell III, J. M., Pumphrey, H. C., Waters, J. W., Bevilacqua, R. M., Kelly, K. K., Hintsa, E. J., Weinstock, E. M., Chiou, E.-W., Chu, W. P., McCormick, M. P., and Webster, C. R.: ATMOS version 3 water vapor measurements: comparisons with observations from two ER-2 Lyman-a hygrometers, MkIV, HALOE, SAGE II, MAS, and MLS, J. Geophys. Res., 107, 4027, doi:10.1029/2001JD000587, 2002.

Mo, K. C.: Relationships between low-frequency variability in the Southern Hemisphere and sea surface temperature anomalies. J. Climate, 13, 3599–3610, 2000.

Murcray, D. G., Murcray, F. J., Barker, D. B., and Mastenbrook, H. J.: Changes in stratospheric water vapor associated with the Mount St. Helens eruption, Science, 211, 823–824, 1981.

Murray, F. W.: On the computation of saturation vapor pressure, J. Appl. Meteorol., 6, 203–204, 1967.

Pieri, D., Ma, C., Simpson, J. J., Hufford, G., Grindle, T., and Grove, C.: Analyses of in-situ airborne volcanic ash from the February 2000 eruption of Hekla Volcano, Iceland, Geophys. Res. Lett., 29, 19-1–19-4, doi:10.1029/2001GL013688, 2002.

ACPD
15, 25873–25905, 2015

Pinto, J. P., Turco, R. P., and Toon, O. B.: Self-limiting physical and chemical effects in volcanic eruption clouds, J. Geophys. Res., 94, 11165–11174, 1989.
Pumphrey, H. C., Read, W. G., Livesey, N. J., and Yang, K.: Observations of volcanic SO_2 from MLS on Aura, Atmos. Meas. Tech., 8, 195–209, doi:10.5194/amt-8-195-2015, 2015.
Randel, W. J., Moyer, E., Park, M., Jensen, E., Bernath, P., Walker, K., and Boone, C.: Global variations of HDO and HDO/H_2O ratios in the upper troposphere and lower stratosphere derived from ACE-FTS satellite measurements, J. Geophys. Res., 117, D06303, doi:10.1029/2011JD016632, 2012.
Rinsland, C. P., Gunson, M. R., Abrams, M. C., Lowes, L. L., Zander, R., Mahieu, E., Goldman, A., Ko, M. K. W., Rodriguez, J. M., and Sze, N. D.: Heterogeneous conversion of N_2O_5 to HNO_3 in the post-Mount Pinatubo eruption stratosphere, J. Geophys. Res., 99, 8213–8219, 1994.
Sears, T. M., Thomas, G. E., Carboni, E., Smith, A. J. A., and Grainger, R. G.: SO_2 as a possible proxy for volcanic ash in aviation hazard avoidance, J. Geophys. Res.-Atmos., 118, 5698–5709, doi:10.1002/jgrd.50505, 2013.
Sioris, C. E., Boone, C. D., Bernath, P. F., Zou, J., McElroy, C. T., and McLinden, C. A.: ACE observations of aerosol in the upper troposphere and lower stratosphere from the Kasatochi volcanic eruption, J. Geophys. Res., 115, D00L14, doi:10.1029/2009JD013469, 2010a.
Sioris, C. E., Zou, J., McElroy, C. T., McLinden, C. A., and Vömel, H.: High vertical resolution water vapour profiles in the upper troposphere and lower stratosphere retrieved from MAESTRO solar occultation spectra, Adv. Space. Res., 46, 642–650, 2010b.
Sioris, C. E., Zou, J., Plummer, D. A., Boone, C. D., McElroy, C. T., Sheese, P. E., Moeini, O., and Bernath, P. F.: Upper tropospheric water vapour variability at high latitudes – Part 1: Influence of the annular modes, Atmos. Chem. Phys. Discuss., 15, 22291–22329, doi:10.5194/acpd-15-22291-2015, 2015.
Soden, B. J., Wetherald, R. T., Stenchikov, G. L., and Robock, A.: Global cooling after the eruption of Mount Pinatubo: a test of climate feedback by water vapor, Science, 296, 727–730, 2002.
Solomon, S., Rosenlof, K. H., Portmann, R. W., Daniel, J. S., Davis, S. M., Sanford, T. J., and Plattner, G.-K.: Contributions of stratospheric water vapor to decadal changes in the rate of global warming, Science, 327, 1219–1223, doi:10.1126/science.1182488, 2010.

ACPD
15, 25873–25905, 2015

Steele, H. M., Eldering, A., and Lumpe, J. D.: Simulations of the accuracy in retrieving stratospheric aerosol effective radius, composition, and loading from infrared spectral transmission measurements, Appl. Optics, 45, 2014–2027, 2006.

Stenke, A. and Grewe, V.: Simulation of stratospheric water vapor trends: impact on stratospheric ozone chemistry, Atmos. Chem. Phys., 5, 1257–1272, doi:10.5194/acp-5-1257-2005, 2005.

Stiller, G. P., Kiefer, M., Eckert, E., von Clarmann, T., Kellmann, S., García-Comas, M., Funke, B., Leblanc, T., Fetzer, E., Froidevaux, L., Gomez, M., Hall, E., Hurst, D., Jordan, A., Kämpfer, N., Lambert, A., McDermid, I. S., McGee, T., Miloshevich, L., Nedoluha, G., Read, W., Schneider, M., Schwartz, M., Straub, C., Toon, G., Twigg, L. W., Walker, K., and Whiteman, D. N.: Validation of MIPAS IMK/IAA temperature, water vapor, and ozone profiles with MOHAVE-2009 campaign measurements, Atmos. Meas. Tech., 5, 289–320, doi:10.5194/amt-5-289-2012, 2012.

Theys, N., De Smedt, I., Van Roozendael, M., Froidevaux, L., Clarisse, L., and Hendrick, F.: First satellite detection of volcanic OClO after the eruption of Puyehue-Cordón Caulle, Geophys. Res. Lett., 41, 667–672, doi:10.1002/2013GL058416, 2014.

Thomason, L. W., Moore, J. R., Pitts, M. C., Zawodny, J. M., and Chiou, E. W.: An evaluation of the SAGE III version 4 aerosol extinction coefficient and water vapor data products, Atmos. Chem. Phys., 10, 2159–2173, doi:10.5194/acp-10-2159-2010, 2010.

Uemera, N., Kuriki, S., Nobuta, K., Yokota, T., Nakajima, H., Sugita, T., and Sasano, Y.: Retrieval of trace gases from aerosol-influenced infrared transmission spectra observed by low-spectral-resolution Fourier-transform spectrometers, Appl. Optics, 44, 455–466, 2005.

Vanhellemont, F., Tetard, C., Bourassa, A., Fromm, M., Dodion, J., Fussen, D., Brogniez, C., Degenstein, D., Gilbert, K. L., Turnbull, D. N., Bernath, P., Boone, C., and Walker, K. A.: Aerosol extinction profiles at 525 nm and 1020 nm derived from ACE imager data: comparisons with GOMOS, SAGE II, SAGE III, POAM III, and OSIRIS, Atmos. Chem. Phys., 8, 2027–2037, doi:10.5194/acp-8-2027-2008, 2008.

Vernier, J.- P., Fairlie, T. D., Murray, J. J., Tupper, A., Trepte, C., Winker, D., Pelon, J., Garnier, A., Jumelet, J., Pavalonis, M., Omar, A. H., and Powell, K. A.: An advanced system to monitor the 3-D structure of diffuse volcanic ash clouds, J. Appl. Meteorol. Clim., 52, 2125–2138, 2013.

Wilcox, L. J., Shine, K. P., and Hoskins, B. J.: Radiative forcing due to aviation water vapour emissions, Atmos. Environ., 63, 1–13, 2012.

ACPD
15, 25873–25905, 2015

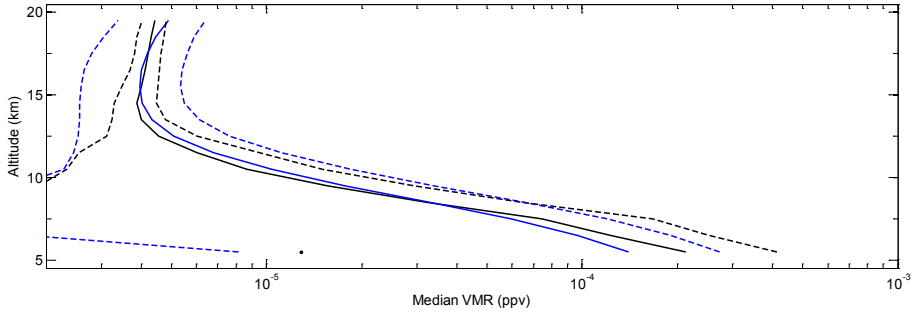

Figure 1. Comparison of global median VMRs from MAESTRO (blue) and ACE-FTS (black). The solid lines are the median profiles while the dashed lines bracket ±1.48 median absolute deviations (MAD) about the median.

ACPD
15, 25873–25905, 2015

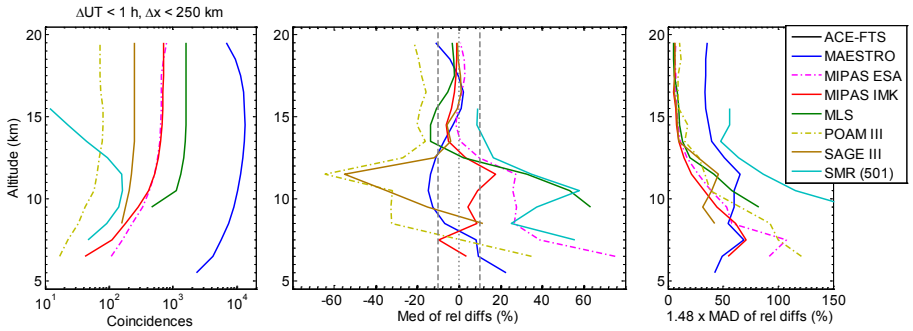

Figure 2. Left: Number of coincidences as a function of altitude between ACE-FTS and various limb sounders that measured water vapour in the ACE time period. The coincidence criteria are < 1 h in time and within 250 km. Centre: Median of relative differences in water vapour vs. ACE-FTS (the minuend). ACE-FTS profiles are assumed to have 3 km vertical resolution and the smoothing accounts for the finite resolution of ACE-FTS and the correlative instruments. ACE-FTS has coarser vertical resolution than most of the chosen instruments. Right: Variability of the relative differences. SAGE is the Stratospheric Aerosol and Gas Experiment. MIPAS IMK is the Michelson Interferometer for Passive Atmospheric Sounding water vapour product developed at the Institut für Meteorologie und Klimaforschung (IMK). The MIPAS water vapour product from the European Space Agency (ESA) is also illustrated. SMR is the sub-mm radiometer on Odin and Aura MLS (Microwave Limb Sounder) is used.

ACPD
15, 25873–25905, 2015

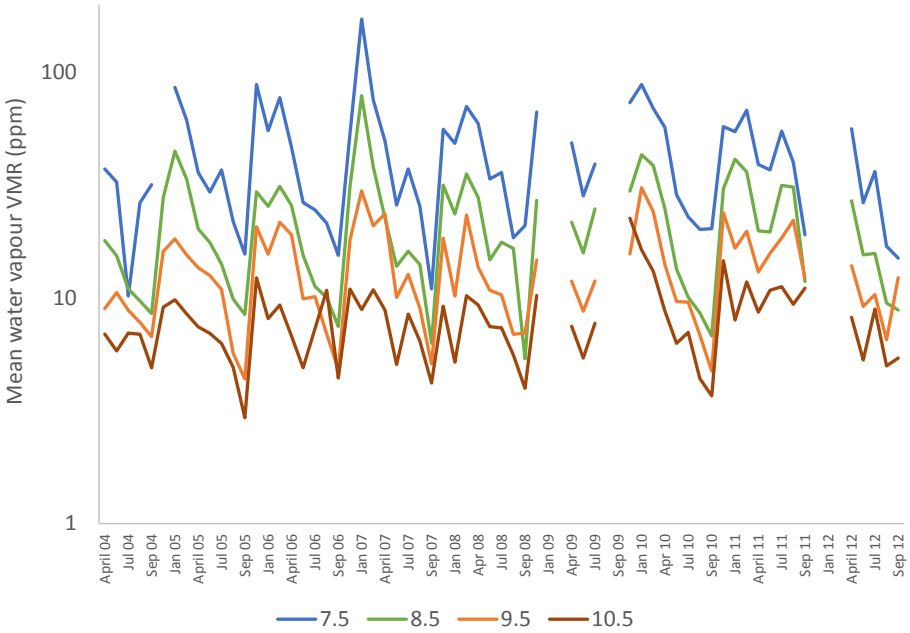

Figure 3. Monthly mean time series of MAESTRO water vapour mixing ratio at different heights (indicated in legend, in km) in the southern high-latitude tropopause region. Months of February, June, October, December are not included as ACE does not sample in this region during those months. Discontinuities indicate insufficient data during the other eight calendar months. A logarithmic scale is used for the *y* axis.

ACPD
15, 25873–25905, 2015

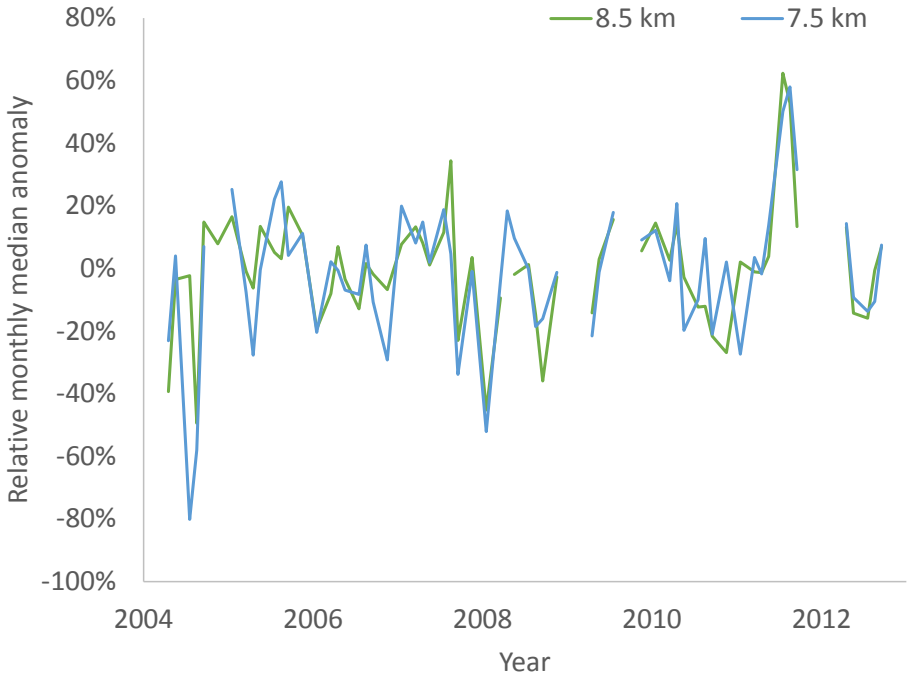

Figure 4. MAESTRO relative monthly median water vapour anomalies at 7.5 and 8.5 km at southern high-latitudes (60–90° S).

ACPD
15, 25873–25905, 2015

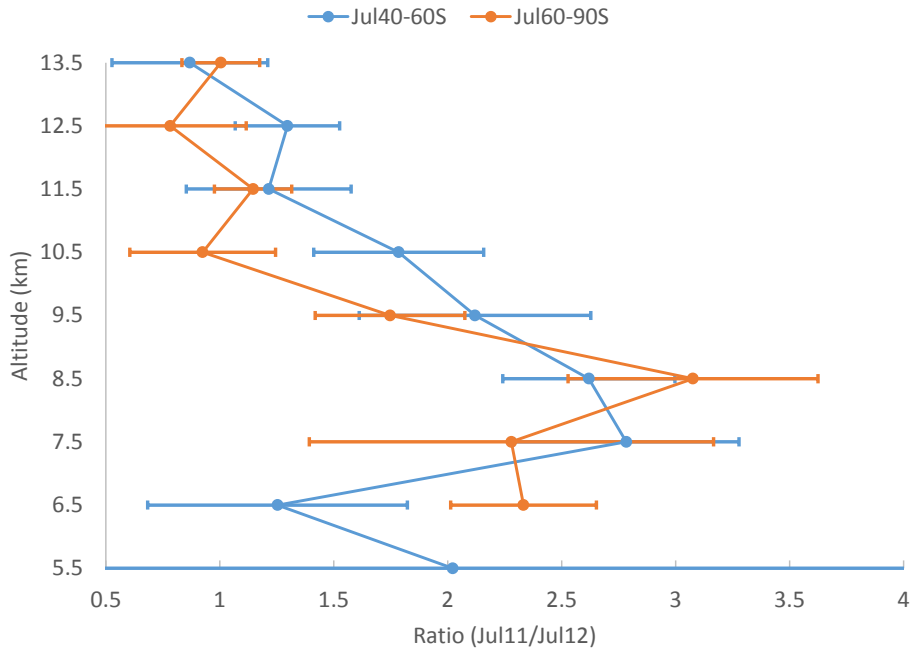

Figure 5. Enhancement factor for water vapour mixing ratio in July 2011 in the 40–60° S band (1 July–12 July) and the 60–66° S band (13 July–31 July), relative to July 2012. The error bar on the ratio profiles account for 1 standard error of the monthly mean for both years, combined in quadrature.

ACPD
15, 25873–25905, 2015

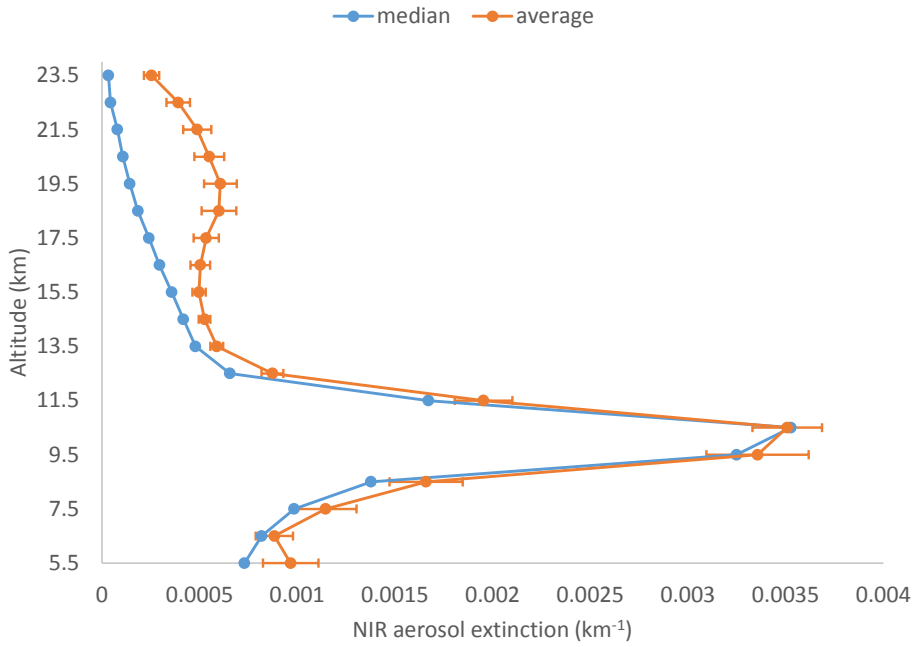

Figure 6. ACE-Imager median and average near-infrared (NIR, 1.02 µm) aerosol extinction profiles for July 2011 at southern high latitudes. The small differences between median and average extinction near the peak indicate a widespread layer in the tropopause region. One standard error of the monthly mean is shown as the error bar.

ACPD
15, 25873–25905, 2015

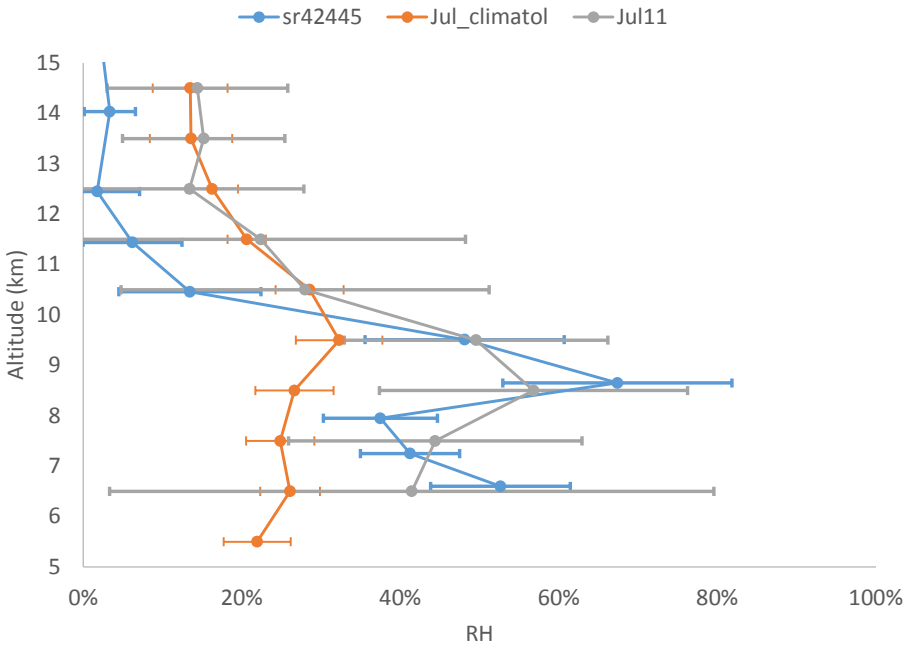

Figure 7. Relative humidity (RH) for sunrise 42 445 (on 1 July 2011 at 42.3° S, see text for details), for July 2011 (60–66° S) and climatology (60–66° S, July for every year of ACE data, except 2011 between 6.5 and 9.5 km) determined from MAESTRO water vapour and GEM pressure and temperature. The error bar for the individual observation accounts for water vapour retrieval uncertainty. The uncertainty on the climatologic RH accounts for interannual variability in water vapour and saturated water vapour mixing ratio, combined in quadrature. The error bar on the July 2011 RH only accounts for the standard error of the monthly mean water vapour.

ACPD
15, 25873–25905, 2015

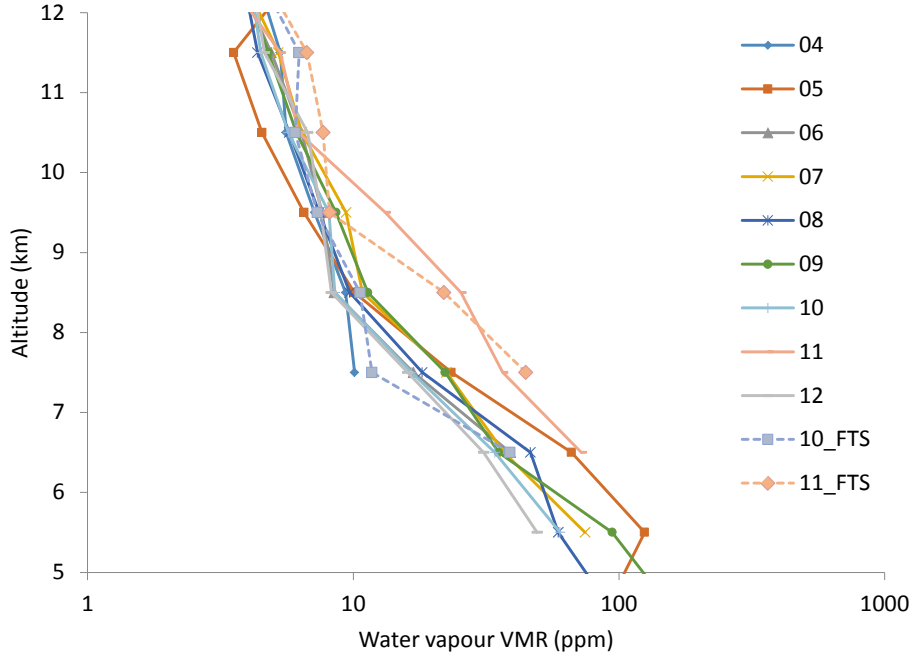

Figure 8. Southern high-latitude (60–90° S) monthly median water vapour profiles in July for different years (MAESTRO: 2004–2012; ACE-FTS: 2010–2011). A logarithmic scale is used for the *x* axis.

ACPD
15, 25873–25905, 2015

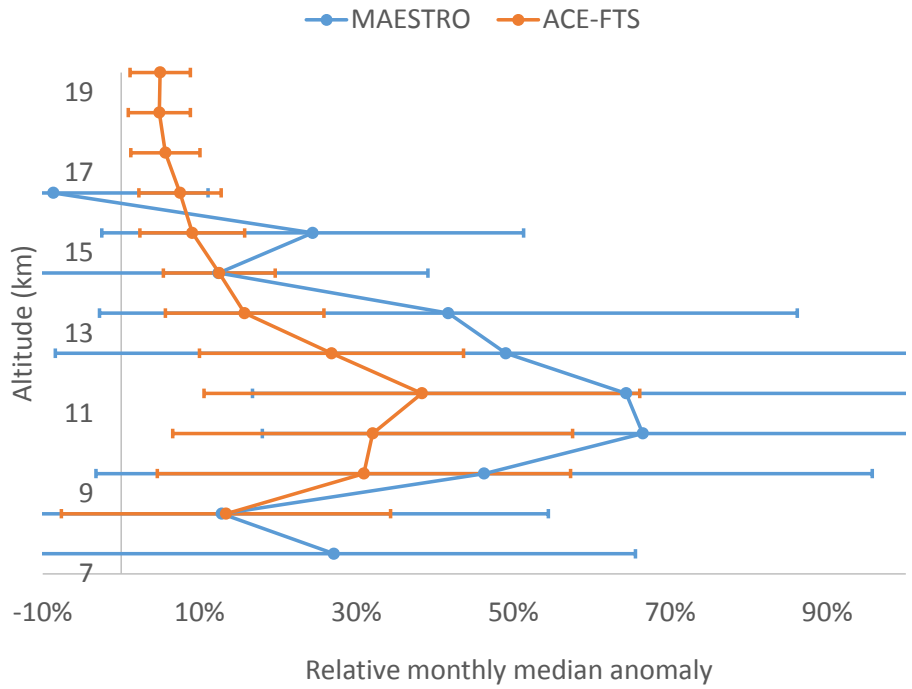

Figure 9. Water vapour relative anomaly at northern high-latitudes in September 2011 (when the stratospheric aerosol optical depth enhancement due to Nabro peaked in this region). The uncertainties reflect the combined natural and instrumental variability (interannual variability (1σ) for September (2004–2012) added in quadrature with the relative standard error of individual September 2011 observations).

ACPD
15, 25873–25905, 2015

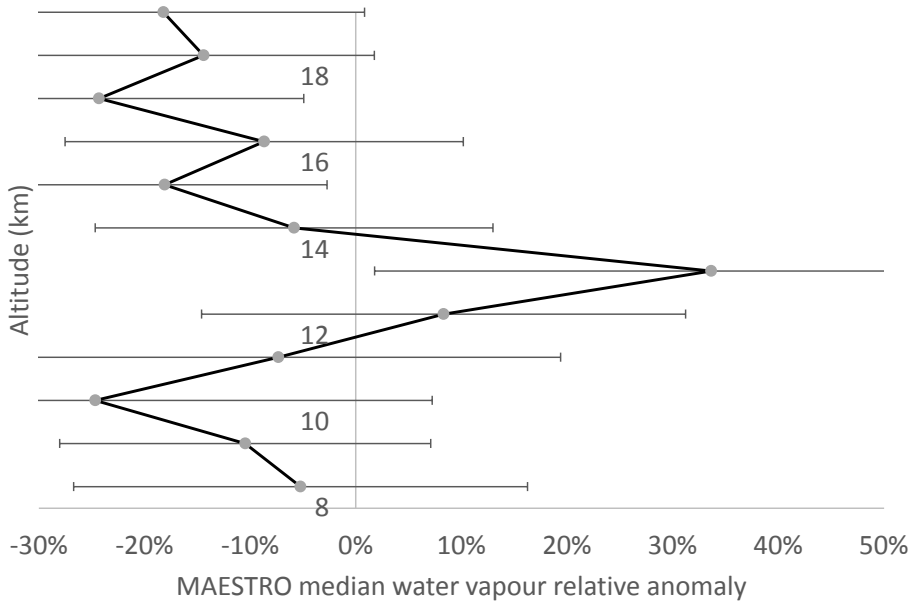

Figure 10. MAESTRO water vapour anomaly at northern mid-latitudes for summer 2011 (average of monthly median anomalies from July and September 2011 data). The uncertainty represents the standard deviation of the July and September anomalies (2004–2012, $12 \leq N \leq 14$, depending on altitude).

ACPD
15, 25873–25905, 2015

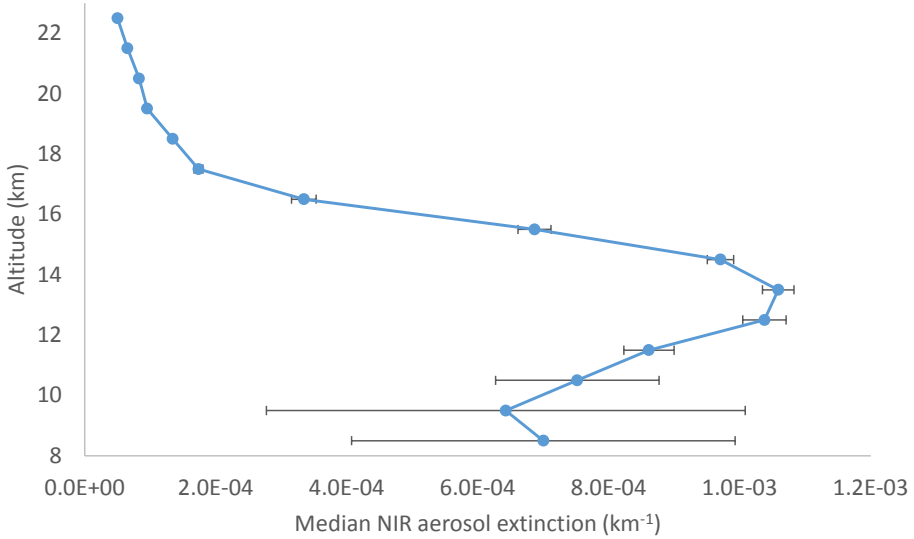

Figure 11. September 2011 median near-infrared aerosol extinction profile for northern high-latitudes based on ACE-Imager observations. The error bar represents the standard error of the monthly mean.

ACPD
15, 25873–25905, 2015

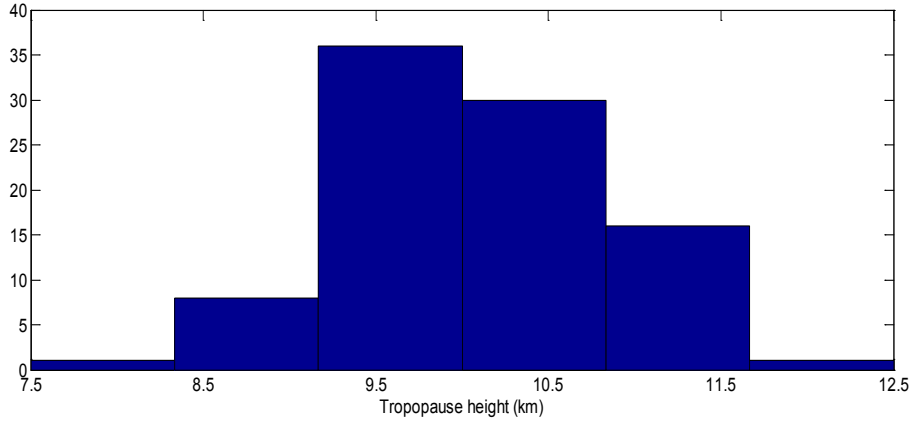

Figure 12. Histogram of tropopause heights in individual soundings in September 2011 at northern high latitudes.

ACPD
15, 25873–25905, 2015

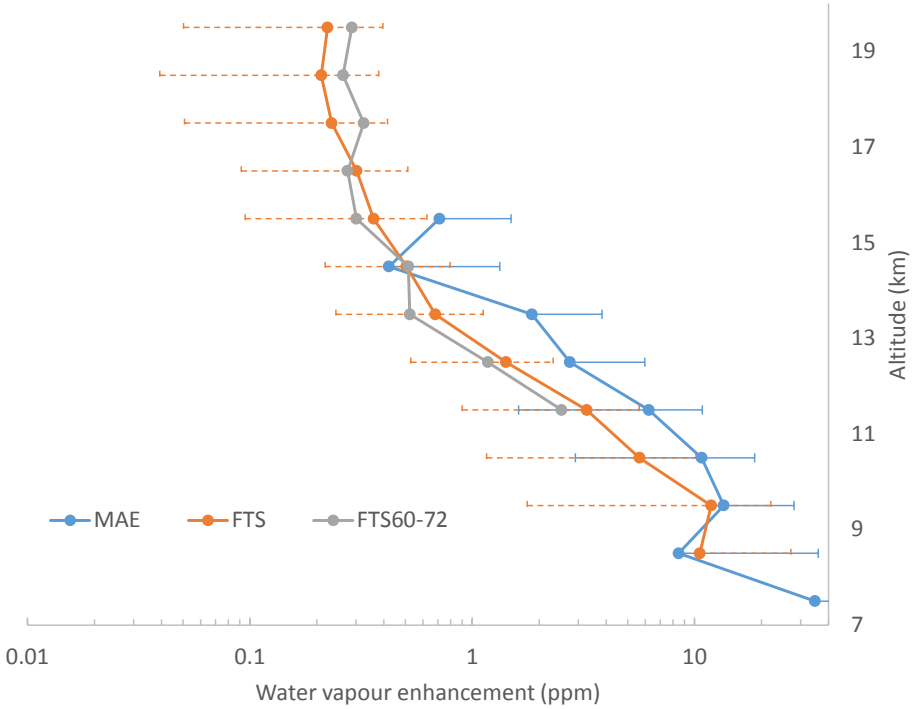

Figure 13. September 2011 median water vapour absolute anomaly based on MAESTRO and ACE-FTS northern high-latitude observations (60–90° N) with the uncertainties accounting for the quadrature sum of the interannual September variability (2005–2012) and the standard error of the individual observations for the month of September 2011 (separately for each instrument). FTS60-72 indicates the anomaly profile for the same time period limiting the observations to a narrower range (60–72° N) which is more uniformly sampled from year-to-year. Uncertainties are missing to the left side of the profile when they exceed 100 %.

ACPD
15, 25873–25905, 2015

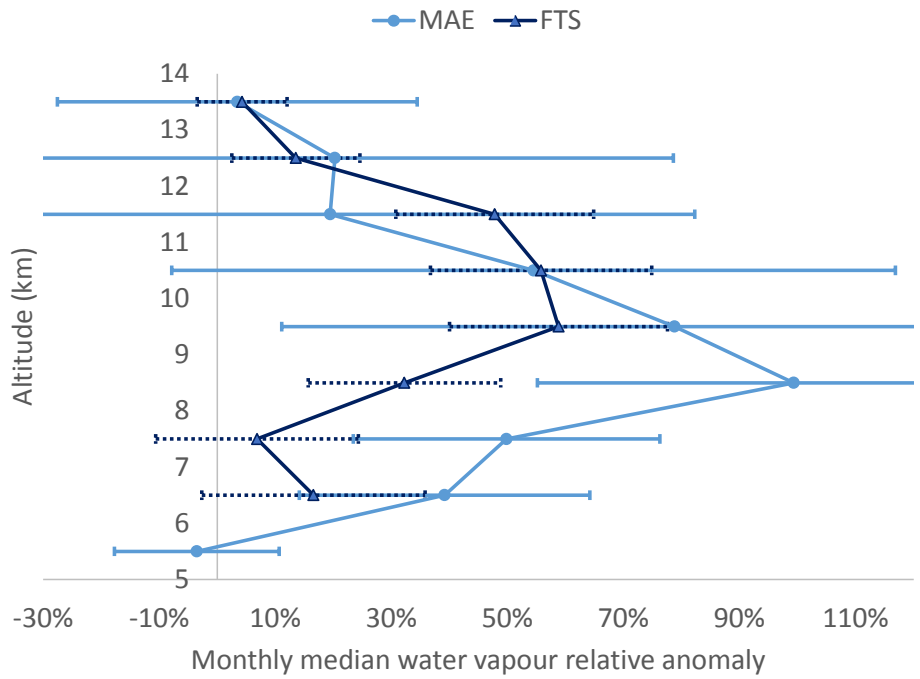

Figure 14. Water vapour relative anomaly in May 2010 at northern high latitudes following the Eyjafjallajökull eruption. The uncertainty accounts for the interannual standard deviation for May (2005–2012) and the relative standard error of individual profiles from the month of May 2010, combined in quadrature.

ACPD
15, 25873–25905, 2015

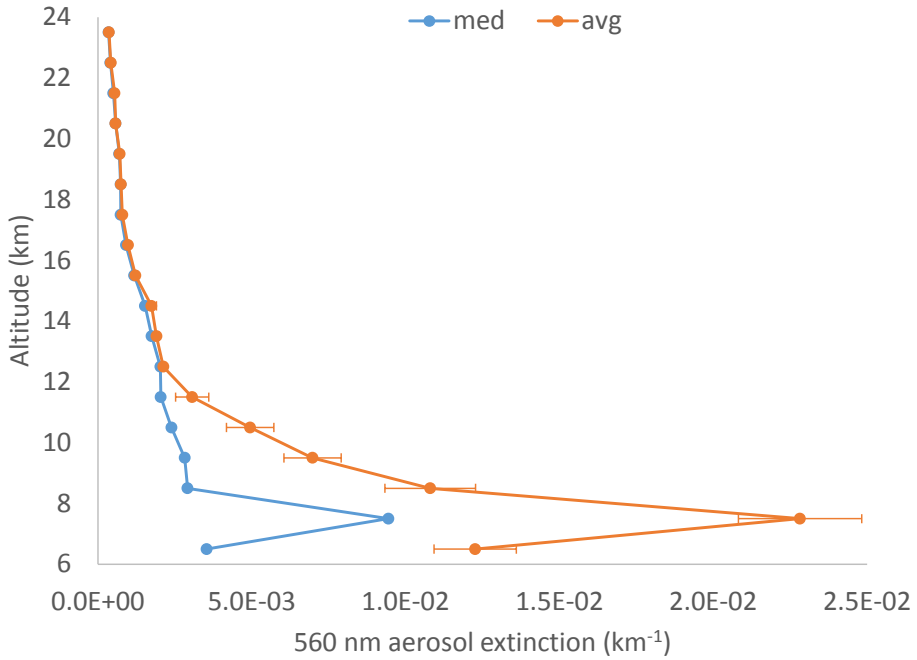

Figure 15. Median and average aerosol extinction observed by MAESTRO at 560 nm in May 2010 at northern high-latitudes.

ACPD
15, 25873–25905, 2015